Large-scale organization of carbon dioxide discharge in the Nepal Himalayas

Frédéric Girault, Laurent Bollinger, Mukunda Bhattarai, Bharat Prasad Koirala, Christian France-Lanord, Sudhir Rajaure, Jérôme Gaillardet, Monique Fort, Soma Nath Sapkota, Frédéric Perrier

Large-scale organization of carbon dioxide discharge in the Nepal Himalayas

Frédéric Girault[1,2], Laurent Bollinger[3], Mukunda Bhattarai[4], Bharat Prasad Koirala[4], Christian France-Lanord[5], Sudhir Rajaure[4], Jérôme Gaillardet[1], Monique Fort[6], Soma Nath Sapkota[4], and Frédéric Perrier[1]

[1]Institut de Physique du Globe de Paris, Sorbonne Paris Cité, Université Paris Diderot, CNRS UMR 7154, Paris, France, [2]Now at Laboratoire de Géologie, École Normale Supérieure, CNRS UMR 8538, Paris, France, [3]CEA, DAM, DIF, Arpajon, France, [4]National Seismological Centre, Department of Mines and Geology, Kathmandu, Nepal, [5]Centre de Recherches Pétrographiques et Géochimiques, Université de Nancy, CNRS UMR 7358, Vandoeuvre-lès-Nancy, France, [6]Département de Géographie, Sorbonne Paris Cité, Université Paris Diderot, CNRS UMR Prodig 8586, Paris, France

Abstract Gaseous carbon dioxide (CO$_2$) and radon-222 release from the ground was investigated along the Main Central Thrust zone in the Nepal Himalayas. From 2200 CO$_2$ and 900 radon-222 flux measurements near 13 hot springs from western to central Nepal, we obtained total CO$_2$ and radon discharges varying from 10^{-3} to 1.6 mol s^{-1} and 20 to 1600 Bq s^{-1}, respectively. We observed a coherent organization at spatial scales of ≈ 10 km in a given region: low CO$_2$ and radon discharges around Pokhara (midwestern Nepal) and in the Bhote Kosi Valley (east Nepal); low CO$_2$ but large radon discharges in Lower Dolpo (west Nepal); and large CO$_2$ and radon discharges in the upper Trisuli Valley (central Nepal). A 110 km long CO$_2$-producing segment, with high carbon isotopic ratios, suggesting metamorphic decarbonation, is thus evidenced from 84.5°E to 85.5°E. This spatial organization could be controlled by geological heterogeneity or large Himalayan earthquakes.

1. Introduction

Convergent zones play an essential role in the global carbon dioxide (CO$_2$) balance of the Earth [*Kerrick and Caldeira*, 1998]. In addition to their role of atmospheric CO$_2$ sink through silicate weathering [*Gaillardet et al.*, 1999; *Gaillardet and Galy*, 2008; *Wolff-Boenisch et al.*, 2009], large orogens are also the location of the production and release of CO$_2$-rich fluids [*Irwin and Barnes*, 1980]. Major active fault zones appear as a complex system where fluid circulation, crustal permeability, and possibly earthquake occurrence might be interrelated dynamically [*Manning and Ingebritsen*, 1999; *Ingebritsen and Manning*, 2010; *Manga et al.*, 2012].

The Himalayas offer a natural laboratory where this essential coupling can be studied. High seismic activity is concentrated on a midcrustal ramp located below the Main Central Thrust (MCT) zone on the Main Himalayan Thrust accommodating the 2 cm yr^{-1} convergence between India and Southern Tibet [*Avouac*, 2003; *Ader et al.*, 2012], where fluid occurrence might explain the high electrical conductivity observed by magnetotelluric sounding [*Lemonnier et al.*, 1999]. Seasonal variations of seismicity [*Bollinger et al.*, 2007] and deformation [*Bettinelli et al.*, 2008; *Chanard et al.*, 2014] can be related to surface hydrological forcing.

Evidence of CO$_2$ release exists in the MCT zone of central Nepal. First, high alkalinity of hot springs up to 56×10^{-3} mol L^{-1} was shown to contribute from 0.5 to 25% to the total dissolved inorganic carbon (DIC) of the entire Narayani watershed [*Evans et al.*, 2004]. Furthermore, the high carbon isotopic ratios (δ^{13}C) of the hot springs, with values reaching +13‰, suggested a metamorphic decarbonation source at depth and a massive CO$_2$ degassing near the water table, larger than 75% in the Trisuli and Marsyandi Valleys [*Becker et al.*, 2008; *Evans et al.*, 2008]. Second, explicit CO$_2$ emission from the ground was discovered near hot springs of the Trisuli Valley, in the Syabru-Bensi hydrothermal system (SBHS) [*Perrier et al.*, 2009], where it was found to be associated with a radon-222 signature and was subsequently mapped in detail [*Girault et al.*, 2014], providing a valuable baseline for long-term monitoring [*Girault et al.*, 2009]. In this paper, we present the results of systematic search and measurement of gaseous CO$_2$ release in the vicinity of other significant hot springs from western to eastern Nepal.
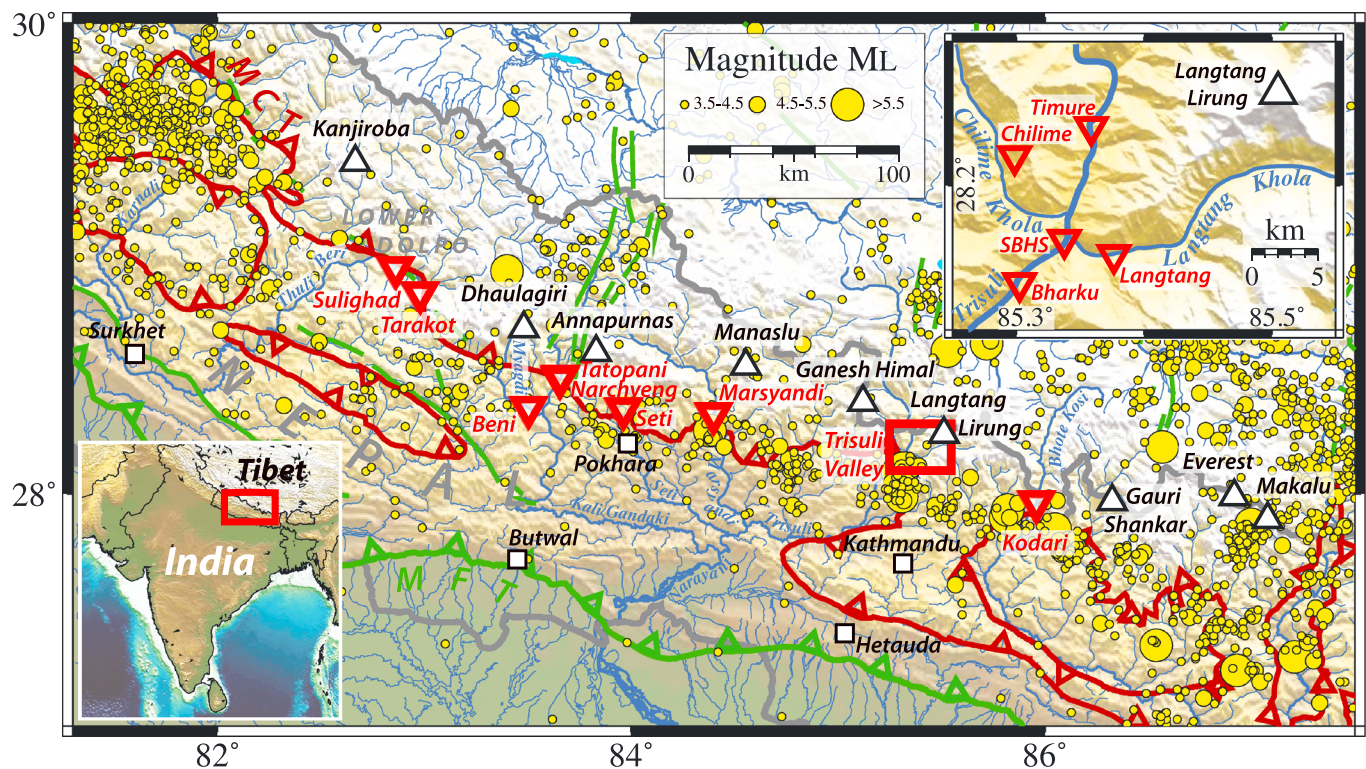
Figure 1. Overview of sites in the Nepal Himalayas. Main Central Thrust (MCT) (brown), Main Frontal Thrust (MFT) faults (green), and highest summits (white triangles) are shown. Earthquake epicenters are taken from the 1994–2012 catalog (Nepal National Seismological Centre) [*Pandey et al.*, 1999]. The bottom left inset shows geographical location. The top right inset shows location of sites in the upper Trisuli Valley. SBHS is the Syabru-Bensi hydrothermal system in central Nepal.

2. Description of the Sites in the MCT Zone

The 2 to 10 km thick MCT shear zone in Nepal (Figure 1), associated with the steep topographic rise of the High Himalayas, places high-grade metamorphic rocks of the Greater Himalayan Sequence over low-grade metamorphic rocks of the Lesser Himalayan Sequence [*Le Fort*, 1975; *Upreti*, 1999]. This region is also characterized by numerous hot springs [*Evans et al.*, 2004].

In this work, we measured the diffuse CO_2 discharge in the vicinity of 13 of these hot springs (Table 1 and Table S1 in the supporting information). All the main hot springs along the Trisuli River in central Nepal were studied (Figure 1, inset): Timure and Chilime, Langtang, and Bharku, located north, east, and south of the SBHS, respectively. Springs located in midwestern Nepal, such as the Myagdi (Beni), Kali Gandaki (Tatopani, Narchyeng), Seti, and Marsyandi Rivers were also examined (Figure 1). This set was complemented (Figure 1) by the Kodari hot spring east of Kathmandu and two hot springs in Lower Dolpo (western Nepal) near tributaries of the Thuli Bheri River: Sulighad near Juphal airport, and Tarakot 20 km eastward.

These hydrothermal systems show various settings (Tables 1, S1, and S2). Kodari, Chilime, Beni, and Tatopani springs, with significant flow rate ($>1\,L\,s^{-1}$), are major pilgrimage and touristic sites. Sulighad, Tarakot, Timure, Bharku, and Langtang springs, with smaller flow rate ($<1\,L\,s^{-1}$), are largely preserved in natural conditions due to their remote location. SBHS, Timure, and Seti springs, with insufficient flow rate to attract much economic activity, show moderate human impacts limited to cemented basins. SBHS, Tatopani, and Chilime sites have pronounced H_2S odor helpful to identify CO_2 degassing [*Girault et al.*, 2009], a signature totally lacking at Sulighad and Tarakot sites despite a similar geological context. At SBHS and Timure sites, several independent CO_2 discharge zones, separated by $>500\,m$, were found.

3. Measurement Methods

At each site, a systematic experimental approach developed in the SBHS was implemented. Methods are briefly recalled here. Details are given in *Girault et al.* [2014].

Table 1. Characteristics of CO_2 and Radon Emission From the Ground

Site	Estimated DIC Discharge From Hot Springs (10^{-3} mol s^{-1})	Diffuse Gaseous CO_2 Discharge							$\delta^{13}C_{gas}$ From CO_2 (PDB) (‰) Mean ± 1σ (Min/Max)
		CO$_2$ Fluxes		Radon Fluxes		Correlation CO$_2$-Radon (Figure 2)	Estimated Global Discharges		
		N [a]	Min–Max Range (g m^{-2} d^{-1})	N [a]	Min–Max Range (10^{-3} Bq m^{-2} s^{-1})	N [b]	CO$_2$ Discharge (10^{-3} mol s^{-1})	Radon Discharge (Bq s^{-1})	
Western Nepal									
Lower Dolpo									
Sulighad	8.4 ± 3.3 [g]	65	1.1–259	50	7.0–3070	44	3.0 ± 0.6	180 ± 40	−10.2 ± 0.1 (−10.2/−10.1)
Tarakot	1.1 ± 0.3 [g]	119	0.8–70	45	0–1410	35	3.8 ± 0.8	70 ± 15	−11.7 ± 0.3
Midwestern Nepal									
Beni	14.1 ± 4.2 [f,g]	49	0.7–35	23	0–27	23	<0.4	<16	n.m.
Kali Gandaki Valley									
Narchyeng	9.7 ± 3.9 [g]	33	1.7–70	18	7.0–111	14	<0.4	<16	n.m.
Tatopani	14.7 ± 4.5 [f,g]	81	0.6–163	36	0–403	36	<0.4	<16	n.m.
Seti	32 ± 16 [f,g]	23	2.4–176	15	0.3–66	15	2.5 ± 0.5	<16	n.m.
Marsyandi	14.1 ± 6.1 [d,e,f,g]	2	2800–3600	0	n.m.	0	>130	n.m.	−2.8 ± 0.1
Central Nepal									
Chilime	15.7 ± 3.3 [d,g]	192	3.4–123,000	61	5.0–3810	59	390 ± 100	290 ± 70	−1.6 ± 0.1
Bharku	n.m.	7	1.9–20	0	n.m.	0	<0.4	n.m.	n.m.
SBHS [c]									
GZ1-2	123 ± 38 [d,f,g]	427	2.5–236,000	184	4.5–38,500	112	900 ± 100	340 ± 70	−0.88 ± 0.09 (−1.3/−0.77)
GZ3	21.1 ± 9.3 [g]	580	2.0–19,000	203	1.2–10,400	82	740 ± 130	1040 ± 210	−0.5 ± 0.1
Total	150 ± 50 [d,f,g]	1314	2.0–236,000	529	1.2–38,500	240	1600 ± 400	1600 ± 300	−0.85 ± 0.09 (−1.3/−0.5)
Timure	12.9 ± 2.6 [d,f,g]	294	0.7–11,100	123	0–1640	114	830 ± 170	840 ± 170	−1.1 ± 0.4 (−1.6/−0.6)
Langtang	0.45 ± 0.14 [f,g]	5	3.5–6.5	0	n.m.	0	<0.4	n.m.	n.m.
Kodari	25 ± 10 [f,g]	5	0–31	0	n.m.	0	<0.4	n.m.	n.m.
Total	**>300 ± 100**	**2189**	**0–236,000**	**900**	**0–38,500**	**580**	**>3000 ± 700**	**>3000 ± 600**	**(−11.7/−0.5)**

[a] Number of CO_2 and radon flux measurements.
[b] Number of measurement points for CO_2-radon correlation (see Figure 2).
[c] Data from the SBHS are detailed in *Girault et al.* [2014].
[d] Data from *Becker* [2005].
[e] Data from *Becker et al.* [2008].
[f] Data from *Evans et al.* [2008].
[g] Data from this study.
n.m.: not measured.

CO_2 and radon fluxes, expressed in g m^{-2} d^{-1} and Bq m^{-2} s^{-1}, respectively, were measured with the accumulation chamber method. After the chamber is installed on the ground, gas concentration was monitored as a function of time, and the initial rate of increase provides a measurement of the flux. The method was tested in detail in the field, and experimental uncertainties were determined to be 5–40% for CO_2 flux and 8–35% for radon flux. An overall common uncertainty of 5% was added quadratically. Mean CO_2 and radon fluxes in background locations without degassing were $16.6 ± 1.3$ g m^{-2} d^{-1} and $0.10 ± 0.02$ Bq m^{-2} s^{-1}, respectively. To obtain the total discharge, expressed in mol s^{-1} or t d^{-1} for CO_2 and Bq s^{-1} or MBq d^{-1} for radon, spatial integration was performed using kriging and interpolation of the available flux data, with uncertainty varying from 10 to 60% as estimated by Monte Carlo simulations.

Sampling of gas and spring water was performed using glass tubes and copper tubes, respectively. Determination of the CO_2 fraction was done manometrically. Carbon isotopic ratios of CO_2 ($\delta^{13}C$, defined relative to the standard values of Pee Dee belemnite, PDB) were obtained by mass spectrometry.

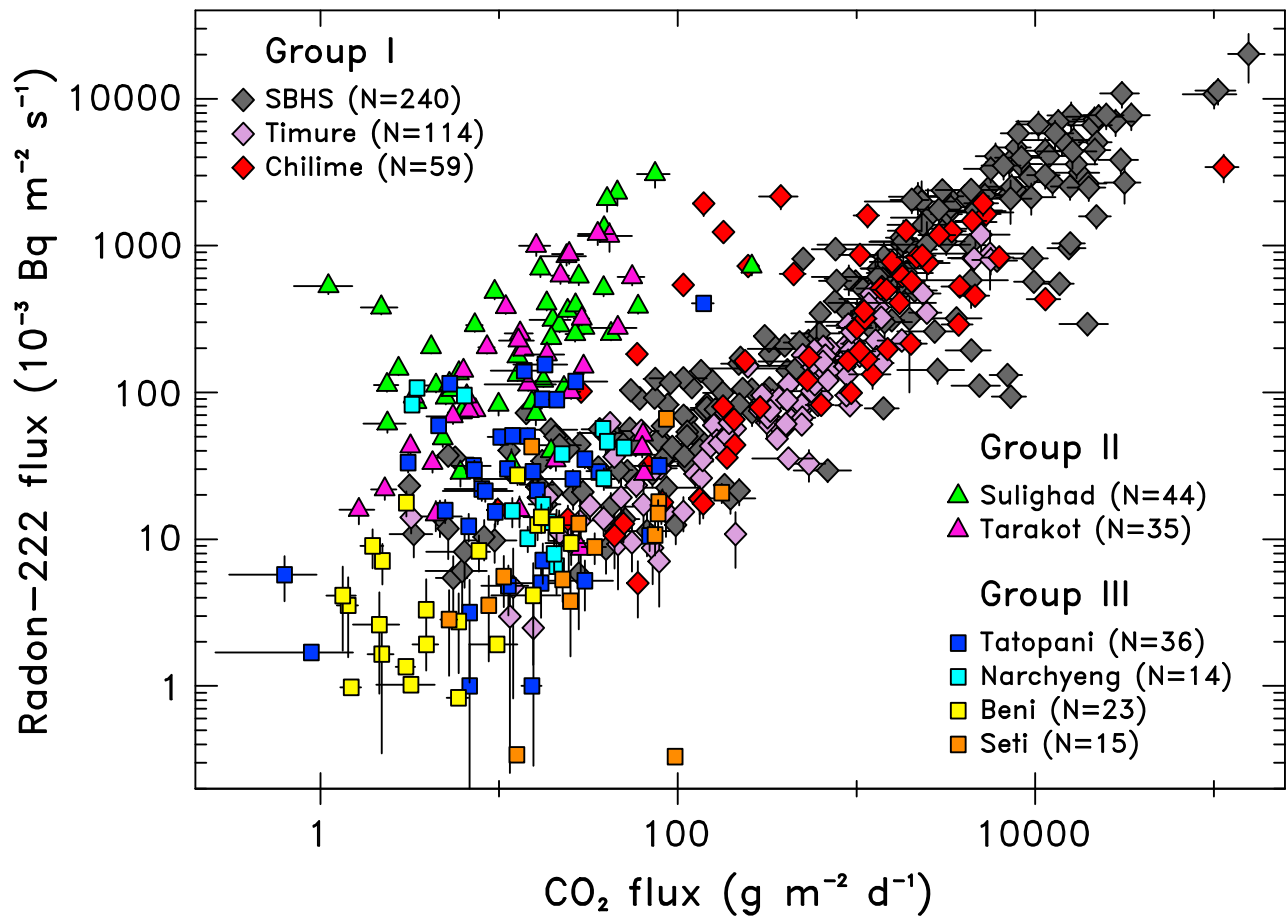**Figure 2.** CO_2 flux versus radon-222 flux.

Radon concentration, expressed in Bq L^{-1}, was systematically measured on site in hot and cold water springs by radon emanometry in air [*Girault and Perrier*, 2014]. Experimental uncertainties were 5–30%. Radium concentration in water, expressed in Bq L^{-1}, was determined in a similar manner in the laboratory.

Methods could not always be applied optimally, owing to several factors (electricity, permission, human impact, and lack of time). Searches were initiated in the immediate vicinity of the hot springs, assisted by infrared thermal imaging. Local people could sometimes indicate suspected gas discharge zones where lethal accidents had occurred.

4. Results

Measurements were carried out during the dry winter seasons between December 2007 and January 2011. Uncertainties correspond to one sigma standard deviation (68% confidence interval), and averages are geometric means.

4.1. CO_2 Flux and Integrated Discharge

A total of 2189 CO_2 and 900 radon fluxes were measured at 580 measurement points (Table 1 and Figure 2). Maximum CO_2 fluxes of 236 ± 50 kg m^{-2} d^{-1} and 123 ± 25 kg m^{-2} d^{-1} were recorded in the SBHS and at Chilime, respectively. Significant CO_2 discharges of 1.6 ± 0.4, 0.83 ± 0.17, and 0.39 ± 0.10 mol s^{-1} were observed at the SBHS, Timure, and Chilime sites, respectively. At Timure, significant discharge was observed despite smaller CO_2 fluxes (maximum of 11.1 ± 2.8 g m^{-2} d^{-1}), due to a larger surface area of CO_2 degassing, extending 150 m from the hot spring on an infrared image (Table S1). Significant CO_2 discharge is thus not a specific feature of the SBHS but is a widespread feature of the upper Trisuli Valley in central Nepal.
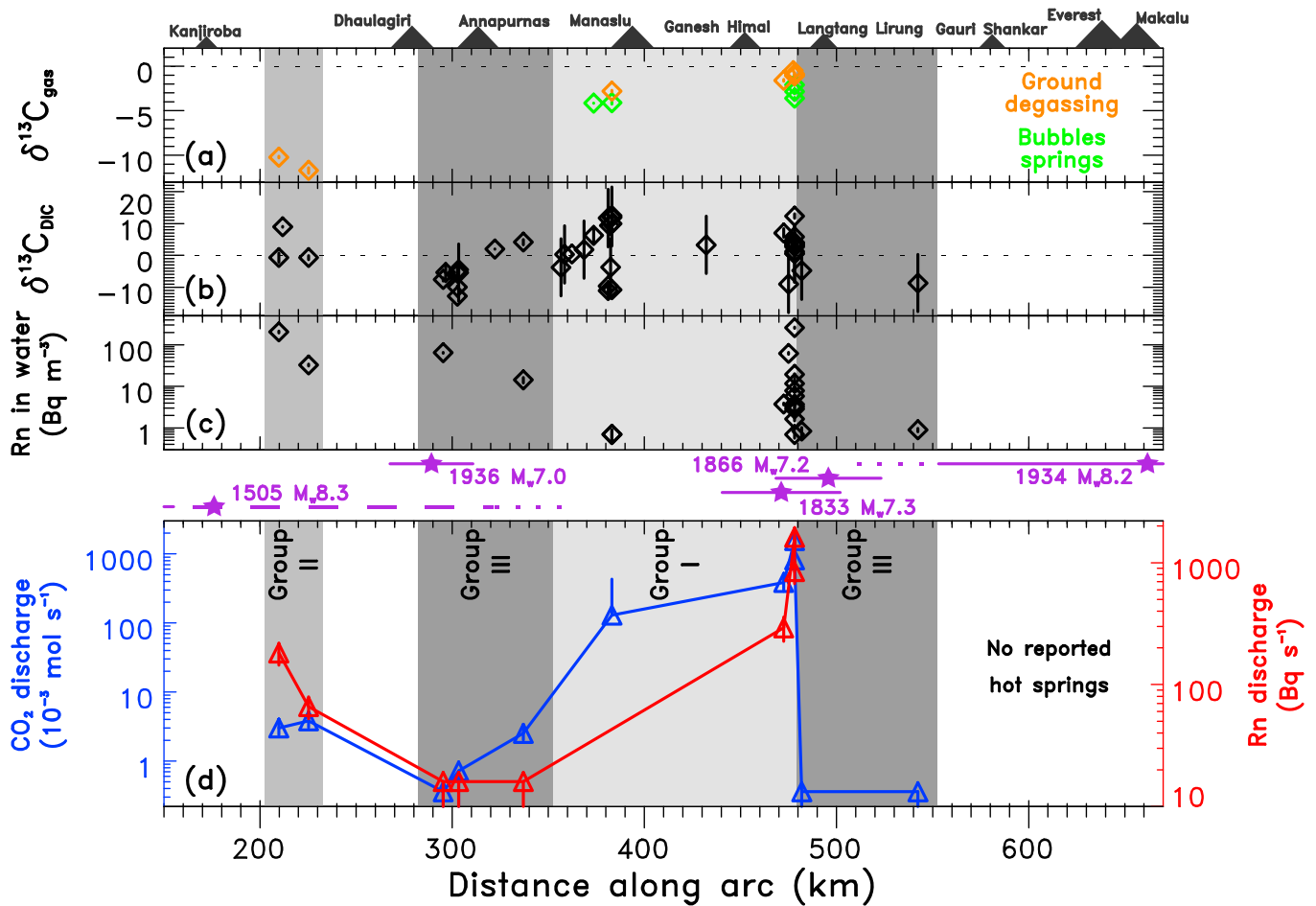
Figure 3. Characteristics of CO_2 degassing from the ground and from water along the Nepal Himalayan arc: (a) Carbon isotope ratios of gaseous CO_2 from the ground and bubbles in springs, (b) carbon isotope ratios of water (dissolved inorganic carbon), (c) radon concentration in spring waters, and (d) CO_2 and radon discharge from the ground (see supporting information). Data are summarized in Tables 1, S1, and S2. Epicenter and rupture lengths of the last significant earthquakes are displayed: the megaquakes of 1505 ($M \geq 8$) [*Ambraseys and Jackson*, 2003] and 1934 ($M_w 8.2$) [*Ambraseys and Douglas*, 2004; *Sapkota et al.*, 2013], and the intermediate earthquakes of 1833 ($M_w 7.3$), 1866 ($M_w 7.2$), and 1936 ($M_w 7.0$) [*Gutenberg and Richter*, 1949; *Szeliga et al.*, 2010].

By contrast, modest CO_2 discharge, similar to background values, was identified southward at Bharku and eastward at Langtang and Kodari. Similarly, in midwestern Nepal, modest CO_2 discharge was observed at Tatopani. Modest CO_2 fluxes were also measured at all sites investigated from Beni to Seti hot springs. In Marsyandi Valley, only two points were measured, but they gave significant flux values (mean of $3200 \pm 300 \, \text{g m}^{-2} \, \text{d}^{-1}$). In western Nepal at Sulighad and Tarakot, maximum CO_2 fluxes from the ground (259 ± 22 and $70 \pm 5 \, \text{g m}^{-2} \, \text{d}^{-1}$) were significantly above local background flux of $6.5 \pm 0.5 \, \text{g m}^{-2} \, \text{d}^{-1}$, but CO_2 discharges are small.

To summarize, substantial CO_2 discharge has thus far only been detected between the Marsyandi and upper Trisuli Valleys, i.e., along a 110 km long region of the Nepal Himalayan belt. Westward and eastward of this region, only low CO_2 discharge, close to background level, was identified (Figure 3).

4.2. Radon Signature of the CO_2 Discharge

Significant radon flux was observed in association with the CO_2 at all sites (Figure 2 and Table 1). Radon fluxes $>1 \, \text{Bq m}^{-2} \, \text{s}^{-1}$, similar to fluxes in the SBHS [*Girault et al.*, 2014], were observed at Timure and Chilime, yielding radon discharges of 840 ± 170 and $290 \pm 70 \, \text{Bq s}^{-1}$, respectively, significant compared with the discharge in the SBHS ($1600 \pm 300 \, \text{Bq s}^{-1}$). In Dolpo, radon discharges were also significant (180 ± 40 and $70 \pm 15 \, \text{Bq s}^{-1}$). Insignificant radon discharge, consistent with the regional background, characterized all other sites.
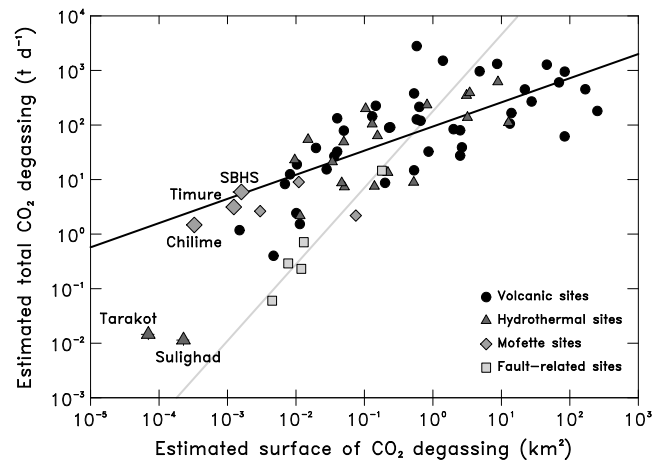
Figure 4. Surface area versus estimated total CO_2 degassing from the ground for our sites together with other selected sites (see review in *Girault et al.* [2014]). Solid lines are power law best fits: black line for volcanic sites and gray line for fault-related sites.

The relationship between radon flux and CO_2 flux varied from site to site (Figures 2 and 3). For example, the case of Dolpo (Sulighad and Tarakot) is conspicuously different, with maximum radon flux reaching 3.1 ± 0.6 and $1.4 \pm 0.2 \, Bq \, m^{-2} \, s^{-1}$, similar to fluxes measured in central Nepal, while the CO_2 flux is relatively low. We therefore propose a classification of the sites based on CO_2 and radon flux data: a first group (group I) with large CO_2 and radon discharges (upper Trisuli Valley including SBHS, Timure, and Chilime, possibly Marsyandi); a second group (group II) with low CO_2 discharge but large radon discharge (Sulighad and Tarakot in Lower Dolpo); and a third group (group III) with low CO_2 and radon discharges (Langtang and Bharku in central Nepal, Kodari to the east, Tatopani, Narchyeng, Beni, and Seti in midwestern Nepal). We did not observe a case of large CO_2 discharge with low radon discharge.

Values of radon concentration in the hot springs confirm this organization (Figure 3 and Table S2): large in Dolpo (205 ± 10 and $33 \pm 2 \, Bq \, L^{-1}$), but small in the hot springs of midwestern and central Nepal ($0.70 \pm 0.18 \, Bq \, L^{-1}$ at Marsyandi, $3.8 \pm 0.2 \, Bq \, L^{-1}$ at Chilime, from 0.7 ± 0.1 to $19 \pm 1 \, Bq \, L^{-1}$ in the SBHS, from 5.8 ± 0.4 to $12 \pm 4 \, Bq \, L^{-1}$ at Timure, and $0.90 \pm 0.09 \, Bq \, L^{-1}$ at Kodari). Except at Langtang and Kodari, radon concentration in water was high when CO_2 discharge was insignificant and low in the presence of large CO_2 discharge.

4.3. Carbon Isotopic Anomalies

In central Nepal, gaseous CO_2 samples showed $\delta^{13}C$ between -1.6 ± 0.1 and -0.5 ± 0.1‰ (mean of -1.2 ± 0.2‰), consistent with previous data which support the concept of a deep metamorphic decarbonation source [*Becker et al.*, 2008; *Evans et al.*, 2008; *Perrier et al.*, 2009]. In Dolpo, similar $\delta^{13}C$ are obtained at both sites, -10.2 ± 0.1 and -11.7 ± 0.3‰, intermediate values between the mean $\delta^{13}C$ of central Nepal and that of biogenic carbon (-25 ± 5‰) [*Cerling*, 1984].

A synthesis of available values of $\delta^{13}C_{DIC}$ for the dissolved inorganic carbon in hot springs is given in Figure 3 and Table S2. Compared with the $\delta^{13}C$ of gas, there was a larger dispersion of $\delta^{13}C_{DIC}$ in water along the Nepal Himalayan belt, ranging from -13.8 to $+13.2$‰. The largest average values were observed in the Marsyandi (12.5‰) [*Becker et al.*, 2008] and upper Trisuli Valleys (12.3 ± 0.7‰) [*Becker*, 2005; *Evans et al.*, 2008].

5. Discussion

We divide the studied sites into three groups, on the basis of CO_2 and radon data (Figures 3 and S1). These must reflect source and transport processes, and a preliminary interpretation is proposed below. In the hydrothermal model of *Becker et al.* [2008] and *Evans et al.* [2008], metamorphic reactions at 10–20 km depth produce CO_2 which percolates through fracture networks, reaching the MCT fault system, where it mixes with meteoric water which eventually is discharged at 60–80°C at the surface. At or near the water table, CO_2 may interact with the atmosphere and degas, enhancing the remnant $\delta^{13}C_{DIC}$. The simplest model for the radon signature is degassing of the radon contained in water [*Girault and Perrier*, 2014]. This model predicts a relationship between radon and CO_2 discharge (Figure S1). For some sites (group II), the radon signature can be accounted for by a small amount of degassing of radon-rich hydrothermal water. By contrast, even when a broad range of conditions are considered (gray band), this model cannot account for the largest CO_2 and radon discharges observed at group I sites Timure and SBHS. The Chilime site appears here intermediate, marginally compatible with simple degassing of radon-bearing water. This analysis indicates that group I is

anomalous and signals the presence of another mechanism, with radon being incorporated at a depth after CO_2 is degassed from water or perhaps suggesting that CO_2 is transported and released independently from hydrothermal circulations [*Girault and Perrier*, 2014]. Differences in the radon flux can be accounted for by different depths of CO_2 degassing or by variations in the effective radium concentration of rocks (i.e., the radon source term) [*Girault et al.*, 2012; *Girault and Perrier*, 2014, Figure 14].

In a given region, sites separated by 5–10 km showed remarkably similar characteristics, suggesting that local topography and hydrology are not major factors controlling the CO_2 heterogeneity. Instead, this consistency indicates a CO_2 source depth of the same typical spatial scale (5 to 10 km). The similar $\delta^{13}C$ of -1.6 ± 0.4‰ points indeed the same CO_2 source, most likely metamorphic decarbonation, over the Nepal Himalayan belt. However, CO_2 emission is modulated along the arc. Indeed, a 110 km long region (Figure 3), which here coincides with group I, showed large CO_2 and radon discharges where hot springs yielded $\delta^{13}C_{DIC} > 10$‰. Outside this region, CO_2 discharge was low, and hot springs gave $\delta^{13}C_{DIC} < -4$‰. Numerous factors might control this large-scale heterogeneity. First, the CO_2 production rate must strongly depend on the available rock material (e.g., the thickness of Greater Himalayan Sequence units), lateral lithology (e.g., along strike changes in lithology, or the lithology of Lesser Himalayan Sequence units), temperature distribution, and other rheological factors associated with MCT activity. Second, the midcrust permeability must affect the CO_2 discharge. A more detailed petrological modeling of the metamorphic reactions [*Groppo et al.*, 2013] is however necessary before the role of permeability can be assessed. Alternative mechanisms for CO_2 production involving sulfuric acid [*Torres et al.*, 2014] may also need to be considered in this case.

The spatial organization of the CO_2 emissions may be discussed also in relation with the distribution of earthquakes. Group II is located in the section of the MCT which shows the least seismic activity over the 1994–2012 time period. This is also (Figure 3) the region covered by the rupture of the large earthquake ($M \geq 8$) of 1505. The eastern group III section is approximately bordered to the east by the 220 km long rupture of the 1934 M_w8.2 Bihar Nepal earthquake [*Sapkota et al.*, 2013; *Bollinger et al.*, 2014], a region where no hot springs are reported. Group I, by contrast, is located in the seismic gap (Figure 3) between the two 1505 and 1934 earthquakes, with smaller major earthquakes ($7 \leq M_w \leq 8$) which have only partially released the accumulated slip deficit since 1505. These relations are unlikely to be coincidental, as Himalayan megaquakes must have a dramatic effect on the large-scale crustal permeability, but the current data are not sufficient to substantiate hypotheses at this stage.

The systems presented in this study are among the first examples of degassing in an active orogen away from volcanic activity. To first order, we can characterize the CO_2 emission by the value of the discharge and the area of the emission, defined as the area with flux larger than $500 \, g \, m^{-2} \, d^{-1}$. In Figure 4, we compare these two parameters for our sites with more familiar instances of mofette sites and a selection of volcanic and hydrothermal sites (reviewed in *Girault et al.* [2014]). The points of group I (SBHS, Timure, and Chilime) with significant discharge over a comparatively small surface area fall at the lower edge of the trend of volcanic and hydrothermal sites. Points of this group therefore are not fundamentally different from volcanic sites, and we can name them "tectonic fumaroles." The contribution of such features, over all active orogens and convergent margins, might not be insignificant compared with active volcanoes. Group II (Sulighad and Tarakot) by contrast, are outside this trend but could be considered as extending the trend of points from major faults.

6. Conclusions

Diffuse CO_2 emissions in the Nepal Himalayas have a remarkably uniform isotopic signature. The accompanying radon signature varies from site to site but shows coherent spatial organization. Over the 350 km long Nepal Himalayan arc that we investigated, significant CO_2 and radon discharges appear concentrated in a 110 km long region spanning about 84.5°E to 85.5°E. We measured a total diffuse CO_2 discharge thus far of $3.0 \pm 0.7 \, mol \, s^{-1}$ (or $11 \pm 3 \, t \, d^{-1}$). This minimum estimate, dominated by three sites located in the upper Trisuli Valley in central Nepal, is larger than the contribution from dissolved inorganic carbon in hot springs ($<0.5 \, mol \, s^{-1}$). This direct observation confirms previous inference [*Becker et al.*, 2008; *Evans et al.*, 2008] that gaseous release of CO_2 dominates the total contribution of the Himalayas, and

this may also be the case in other active orogens. The observed heterogeneity, however, makes extrapolation to a whole chain from a few sites particularly difficult.

This study can only be considered a first step toward obtaining a reliable estimate of CO_2 release by the Himalayas. Degassing has not yet been studied in large areas of the Nepal Himalayas, including the far western region characterized by an intense seismic activity (Figure 1) and the eastern region East from Makalu. No CO_2 emissions have been measured so far in India, Bhutan, or Pakistan. In western Nepal, the region from Marsyandi Valley to Ganesh Himal deserves more detailed mapping. Furthermore, we have sometimes observed degassing away from the hot springs along the MCT, at Timure or in the SBHS, for example, and our ability to measure large CO_2 fluxes was due to the use of infrared images or an element of luck.

The origin of the CO_2 released in the Nepal Himalayas, while likely metamorphic, remains insufficiently constrained. A better understanding of the source, including petrological [*Groppo et al.*, 2013] and thermomechanical modeling [*Bollinger et al.*, 2006], is mandatory before transport properties of the MCT zone can be assessed. The spatial distribution of our data suggests that in the future some attention should definitely be given to relationships between CO_2 emissions, deformation, and Himalayan earthquakes. The presence of different types of diffuse CO_2 emissions makes the Himalayas a unique natural laboratory where, for example, a dynamic connection between crust permeability and the earthquake cycle [*Ingebritsen et al.*, 2006] can be studied. Such working hypotheses may have important consequences in terms of coseismic or preseismic gas bursts.

References

Ader, T., et al. (2012), Convergence rate across the Nepal Himalaya and interseismic coupling on the Main Himalayan Thrust: Implications for seismic hazard, *J. Geophys. Res.*, *117*, B04403, doi:10.1029/2011JB009071.

Ambraseys, N. N., and D. Jackson (2003), A note on early earthquakes in northern India and southern Tibet, *Curr. Sci. India*, *84*, 570–582.

Ambraseys, N. N., and J. Douglas (2004), Magnitude calibration of north Indian earthquakes, *Geophys. J. Int.*, *159*(1), 165–206.

Avouac, J.-P. (2003), Mountain building, erosion, and the seismic cycle in the Nepal Himalaya, *Adv. Geophys.*, *46*, 1–80.

Becker, J. A. (2005), Quantification of Himalayan metamorphic CO_2 fluxes: Impact on global carbon budgets, PhD thesis, Univ. of Cambridge, Cambridge, U. K.

Becker, J. A., M. J. Bickle, A. Galy, and T. J. B. Holland (2008), Himalayan metamorphic CO_2 fluxes: Quantitative constraints from hydrothermal springs, *Earth Planet. Sci. Lett.*, *265*, 616–629.

Bettinelli, P., J.-P. Avouac, M. Flouzat, L. Bollinger, G. Ramillien, S. Rajaure, and S. Sapkota (2008), Seasonal variations of seismicity and geodetic strain in the Himalaya induced by surface hydrology, *Earth Planet. Sci. Lett.*, *266*, 332–344.

Bollinger, L., P. Henry, and J.-P. Avouac (2006), Mountain building in the Nepal Himalaya: Thermal and kinematic model, *Earth Planet. Sci. Lett.*, *244*, 58–71.

Bollinger, L., F. Perrier, J.-P. Avouac, S. Sapkota, U. Gautam, and D. R. Tiwari (2007), Seasonal modulation of seismicity in the Himalaya of Nepal, *Geophys. Res. Lett.*, *34*, L08304, doi:10.1029/2006GL029192.

Bollinger, L., S. N. Sapkota, P. Tapponnier, Y. Klinger, M. Rizza, J. Van der Woerd, D. R. Tiwari, and R. Pandey (2014), Estimating the return times of great Himalayan earthquakes in Eastern Nepal: Evidence from the Patu and Bardibas strands of the Main Frontal Thrust, *J. Geophys. Res. Solid Earth*, doi:10.1002/2014JB010970.

Cerling, T. E. (1984), The stable isotope composition of modern soil carbonate and its relationship to climate, *Earth Planet. Sci. Lett.*, *71*, 229–240.

Chanard, K., J.-P. Avouac, G. Ramilien, and J. Genrich (2014), Modeling deformation induced by seasonal variations of continental water in the Himalaya region: Sensitivity to Earth elastic structure, *J. Geophys. Res. Solid Earth*, *119*, 5097–5113, doi:10.1002/2013JB010451.

Evans, M. J., L. A. Derry, and C. France-Lanord (2004), Geothermal fluxes of alkalinity in the Narayani river system of central Nepal, *Geochem. Geophys. Geosyst.*, *5*, Q08011, doi:10.1029/2004GC000719.

Evans, M. J., L. A. Derry, and C. France-Lanord (2008), Degassing of metamorphic carbon dioxide from the Nepal Himalaya, *Geochem. Geophys. Geosyst.*, *9*, Q04021, doi:10.1029/2007GC001796.

Gaillardet, J., and A. Galy (2008), Himalaya—Carbon sink or source?, *Science*, *320*, 1727–1728.

Gaillardet, J., B. Dupré, P. Louvat, and C. J. Allègre (1999), Global silicate weathering and CO_2 consumption rates deduced from the chemistry of large rivers, *Chem. Geol.*, *159*, 3–30.

Girault, F., and F. Perrier (2014), The Syabru-Bensi hydrothermal system in central Nepal: 2. Modeling and significance of the radon signature, *J. Geophys. Res. Solid Earth*, *119*, 4056–4089, doi:10.1002/2013JB010302.

Girault, F., B. P. Koirala, F. Perrier, P. Richon, and S. Rajaure (2009), Persistence of radon-222 flux during monsoon at a geothermal zone in Nepal, *J. Environ. Radioact.*, *100*, 955–964.

Girault, F., F. Perrier, A. P. Gajurel, M. Bhattarai, B. P. Koirala, L. Bollinger, M. Fort, and C. France-Lanord (2012), Effective radium concentration across the Main Central Thrust in the Nepal Himalayas, *Geochim. Cosmochim. Acta*, *98*, 203–227.

Girault, F., et al. (2014), The Syabru-Bensi hydrothermal system in central Nepal: 1. Characterization of carbon dioxide and radon fluxes, *J. Geophys. Res. Solid Earth*, *119*, 4017–4055, doi:10.1002/2013JB010301.

Groppo, C., F. Rolfo, D. Castelli, and J. A. D. Connolly (2013), Metamorphic CO_2 production from calc-silicate rocks via garnet-forming reactions in the CFAS–H_2O–CO_2 system, *Contrib. Mineral. Petrol.*, *166*, 1655–1675.

Gutenberg, B., and C. F. Richter (1949), *Seismicity of the Earth and Associated Phenomena*, 295 pp., Princeton Univ. Press, Princeton, N. J.

Ingebritsen, S. E., and C. E. Manning (2010), Permeability of the continental crust: Dynamic variations inferred from seismicity and metamorphism, *Geofluids*, *10*, 193–205.

Ingebritsen, S. E., W. E. Sanford, and C. E. Neuzil (2006), *Groundwater in Geologic Processes*, 2nd ed., 536 pp., Cambridge Univ. Press, Cambridge, U. K.

Irwin, W. P., and I. Barnes (1980), Tectonic relations of carbon dioxide discharges and earthquakes, *J. Geophys. Res.*, *85*(B6), 3115–3121, doi:10.1029/JB085iB06p03115.

Kerrick, D. M., and K. Caldeira (1998), Metamorphic CO_2 degassing from orogenic belts, *Chem. Geol.*, *145*, 213–232.

Le Fort, P. (1975), Himalayas: Collided range, present knowledge of continental arc, *Am. J. Sci.*, *A275*, 1–44.

Lemonnier, C., G. Marquis, F. Perrier, J.-P. Avouac, G. Chitrakar, B. Kafle, S. Sapkota, U. Gautam, D. Tiwari, and M. Bano (1999), Electrical structure of the Himalaya of Central Nepal: High conductivity around the mid-crustal ramp along the MHT, *Geophys. Res. Lett.*, *26*(21), 3261–3264, doi:10.1029/1999GL008363.

Manga, M., I. Beresnev, E. E. Brodsky, J. E. Elkhoury, D. Elsworth, S. E. Ingebritsen, D. C. Mays, and C.-Y. Wang (2012), Changes in permeability caused by transient stresses: Field observations, experiments, and mechanisms, *Rev. Geophys.*, *50*, RG2004, doi:10.1029/2011RG000382.

Manning, C. E., and S. E. Ingebritsen (1999), Permeability of the continental crust: Implications of geothermal data and metamorphic systems, *Rev. Geophys.*, *37*(1), 127–150, doi:10.1029/1998RG900002.

Pandey, M. R., R. P. Tandukar, J.-P. Avouac, J. Vergne, and T. Héritier (1999), Seismotectonics of the Nepal Himalaya from a local seismic network, *J. Asian Earth Sci.*, *17*, 703–712.

Perrier, F., et al. (2009), A direct evidence for high carbon dioxide and radon-222 discharge in Central Nepal, *Earth Planet. Sci. Lett.*, *278*, 198–207.

Sapkota, S. N., L. Bollinger, Y. Klinger, P. Tapponnier, Y. Gaudemer, and D. Tiwari (2013), Primary surface ruptures of the great Himalayan earthquakes in 1934 and 1255, *Nat. Geosci.*, *6*, 71–76.

Szeliga, W., S. Hough, S. Martin, and R. Bilham (2010), Intensity, magnitude, location, and attenuation in India for felt earthquakes since 1762, *B. Seismol. Soc. Am.*, *100*(2), 570–584.

Torres, M. A., A. J. West, and G. Li (2014), Sulphide oxidation and carbonate dissolution as a source of CO_2 over geological timescales, *Nature*, *507*, 346–349.

Upreti, B. N. (1999), An overview of the stratigraphy and tectonics of the Nepal Himalaya, *J. Asian Earth Sci.*, *17*, 577–606.

Wolff-Boenisch, D., E. J. Gabet, D. W. Burbank, H. Langner, and J. Putkonen (2009), Spatial variations in chemical weathering and CO_2 consumption in Nepalese High Himalayan catchments during the monsoon season, *Geochim. Cosmochim. Acta*, *73*, 3148–3170.